doi:10.1016/j.jmb.2010.11.023 J. Mol. Biol. (2011) 405, 1154–1169

Contents lists available at www.sciencedirect.com

Journal of Molecular Biology

journal homepage: http://ees.elsevier.com.jmb

# Active Mutants of the TCR-Mediated p38α Alternative Activation Site Show Changes in the Phosphorylation Lip and DEF Site Formation

**Netanel Tzarum, Ron Diskin, David Engelberg and Oded Livnah***

*Department of Biological Chemistry, Alexander Silberman Institute of Life Sciences, Hebrew University of Jerusalem, Jerusalem 91904, Israel*
*Wolfson Centre for Applied Structural Biology, Hebrew University of Jerusalem, Jerusalem 91904, Israel*

*Received 7 September 2010; received in revised form 8 November 2010; accepted 10 November 2010*
Available online 10 December 2010

***Edited by I. Wilson***

***Keywords:***
MAP kinase;
p38α;
T-cells;
signaling;
alternative activation

The p38α mitogen-activated protein kinase is commonly activated by dual (Thr and Tyr) phosphorylation catalyzed by mitogen-activated protein kinase kinases. However, in T-cells, upon stimulation of the T-cell receptor, p38α is activated via an alternative pathway, involving its phosphorylation by zeta-chain-associated protein kinase 70 on Tyr323, distal from the phosphorylation lip. Tyr323-phosphorylated p38α is autoactivated, resulting in monophosphorylation of Thr180. The conformational changes induced by pTyr323 mediating autoactivation are not known. The lack of pTyr323 p38α for structural studies promoted the search for Tyr323 mutations that may functionally emulate its effect when phosphorylated. Via a comprehensive mutagenesis of Tyr323, we identified mutations that rendered the kinase intrinsically active and others that displayed no activity. Crystallographic studies of selected active ($p38\alpha^{Y323Q}$, $p38\alpha^{Y323T}$, and $p38\alpha^{Y323R}$) and inactive ($p38\alpha^{Y323F}$) mutants revealed that substantial changes in interlobe orientation, extended conformation of the activation loop, and formation of substrate docking DEF site (docking site for extracellular signal-regulated kinase FXF) interaction pocket are associated with p38α activation.



## Introduction

The p38 kinases are a subgroup of the mitogen-activated protein kinase (MAPK) enzymes[1] that also include extracellular signal-regulated kinases (ERKs), big MAPKs, and c-Jun N-terminal kinases. The p38 subfamily consists of four isoforms, α, β, γ, and δ, which share a high level of sequence similarity[2] but differ in how they are recognized by various MAPK kinases (MKKs)[3] and in their tissue expression pattern.[4] These serine/threonine kinases participate in various cellular processes including inflammatory responses, differentiation, cell death, senescence, and tumor suppression.[5–7] Abnormal activity of p38 is associated with various diseases including chronic inflammatory diseases,[8,9] psoriasis, and cancer,[10–13] making it a viable target for drug design.[10–16]

The p38 enzymes are catalytically activated when cells experience extracellular stimuli, commonly stress signals including osmotic shock and UV radiation and biological signals such as growth

*Corresponding author. Department of Biological Chemistry, Alexander Silberman Institute of Life Sciences, Hebrew University of Jerusalem, Safra Campus, Givat Ram, Jerusalem 91904, Israel. E-mail address: oded.livnah@huji.ac.il.

Abbreviations used: MAPK, mitogen-activated protein kinase; ERK, extracellular signal-regulated kinase; MKK, MAPK kinase; MKI, MAPK insert; ATF, activating transcription factor; β-OG, *n*-octyl-β-D-glucopyranoside; ESRF, European Synchrotron Radiation Facility; PDB, Protein Data Bank; ZAP-70, zeta-chain-associated protein kinase 70; DEF site, docking site for ERK FXF.

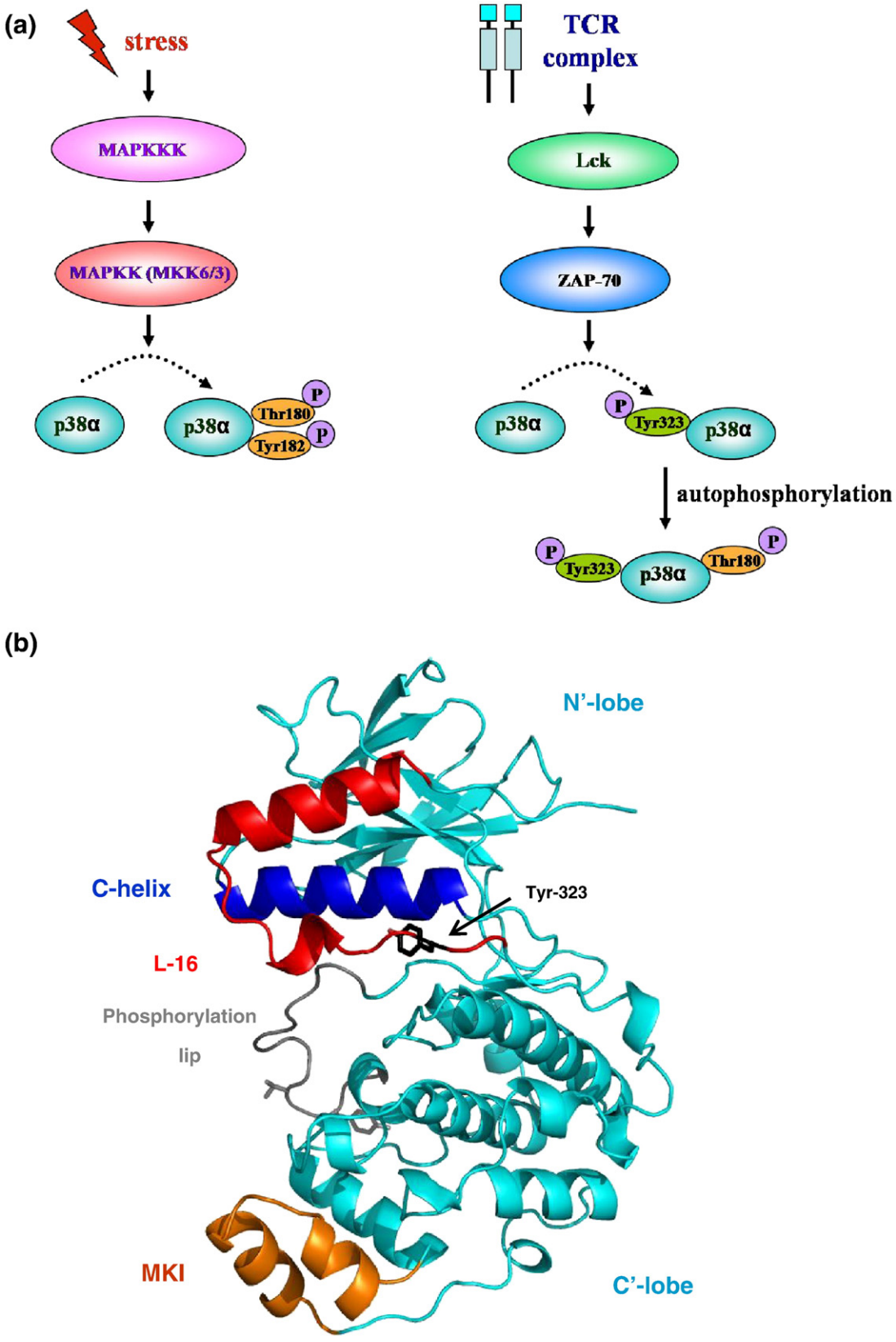


**Fig. 1** (*legend on next page*)

and inflammatory factors.[8,9,17–21] These stimuli activate specific sensors and receptors that transduce the signal to the cytoplasmic components. Many of the signals ultimately reach the MAPK system whose core comprises three kinases that successively phosphorylate and activate each other (MKK kinase, MKK, and MAPK)[22] (Fig. 1a). The most upstream kinase in this three-tiered hierarchy is a member of the MKK kinase group, which, in turn, phosphorylates and activates members of the MKK family. MKKs are dual-specificity Thr and Tyr kinases that phosphorylate their substrates, MAPKs, on a unique Thr-Xaa-Tyr motif located on the activation loop (also termed phosphorylation lip). Once dually phosphorylated, MAPKs become catalytically active and are capable of phosphorylating numerous substrates in the cytosol and nucleus.[24]

MKK-dependent phosphorylation was considered the sole activation mechanism of MAPK catalysis,[1] yet three alternative activation mechanisms have been described for p38: (1) Activating p38α in response to transforming growth factor-β signaling by a direct interaction with transforming growth factor-β-activated protein kinase 1 binding protein 1 (TAB1). This interaction leads to autophosphorylation, which activates p38α.[25] (2) Activation via binding to phosphatidylinositol analogues, which induces p38α autophosphorylation.[26] (3) Activation via phosphorylation of Tyr323, distal from the canonic phosphorylation sites on the activation loop.[27] Tyr323 phosphorylation leads to p38α autophosphorylation solely on Thr180 of the Thr-Gly-Tyr motif and to subsequent activation of p38α.[28] This mechanism is exclusive to T-cells and is induced following T-cell receptor activation and recruitment of the tyrosine kinase Lck and zeta-chain-associated protein kinase 70 (ZAP-70) that ultimately phosphorylates p38α/p38β on Tyr323[27] (Fig. 1a). The MKK-independent phospho-Tyr323-invoked pathway is essential for producing cytokines, such as interferon-γ, in response to T-cell receptor activation,[29] although the canonic MKK-dependent p38 activation pathway is also functional in T-cells. Moreover, the Thr-monophosphorylated, Tyr323-activated p38 was shown to have a substrate selectivity different from that of the dually phosphorylated p38.[28]

It is not known which conformational changes induced by Tyr323 phosphorylation lead to autophosphorylation. Available structures of p38s and other MAPKs have an overall topology similar to that of the canonical protein kinase structure, which consists of two lobes (N′ and C′) that form the catalytic groove between them[30] (Fig. 1b). The phosphorylation lip bearing the phosphoacceptors is also located between the lobes. The MAPK insert (MKI) region, unique in MAPKs, is located at the edge of the C′-lobe.[31] The lobes are linked by two segments (residues 107–113 and 305–320 in p38α) that allow flexibility upon activation and/or substrate binding. The latter segment bears the common docking domain (residues 313–316), which dictates molecular recognition toward upstream activators, substrates, and phosphatases.[32–34] The DEF site (docking site for ERK FXF) interaction pocket on the C′-lobe of certain MAPKs is a secondary docking site.[32,35,36] The DEF site interaction pocket of ERK2 is formed upon phosphorylation[37] and can accommodate aromatic/hydrophobic residues proximal to the substrate phosphoacceptor. Another distinctive feature of MAPKs is the C-terminal extension consisting of a loop (L16) region (residues 321–334, p38α numbering) followed by helix 16. Here, the L16 loop region is a continuation of the second kinase interlobe linker.

Tyr323, located in the L16 loop region, is conserved in p38α, p38β, and p38γ. However, p38δ and the yeast ortholog, Hog1, have a phenylalanine residue in the equivalent position (Phe324 and Phe318, respectively) (Supplemental Fig. 1). Mutating this Phe in Hog1 or p38δ results in intrinsic (MKK-independent) autophosphorylation and catalytic activity.[38,39] Autophosphorylation and autoactivation also occur in p38α when Phe327, adjacent to Tyr323, is mutated to Ser or Leu.[40] Their corresponding crystal structures displayed local conformational changes, suggesting that similar changes may occur naturally when Tyr323 is phosphorylated.[41]

The pivotal role of pTyr323 in inducing autophosphorylation and autoactivation, combined with the structural data of the intrinsically active p38α$^{F327L}$ and p38α$^{F327S}$, suggests that manipulating Tyr323 could induce autophosphorylation of p38α and

**Fig. 1.** p38 activation pathways and structure. (a) Schematic diagram of the canonic three-stage MAPK activation pathway, which results in dual phosphorylation on neighboring Thr180 and Tyr182 residues (p38α numbering) located on the phosphorylation lip (left). An alternative p38 activation pathway, exclusive in T-cells, which results in phosphorylation of p38α/p38β on Tyr323, by the ZAP-70 tyrosine kinase (right). Subsequent to Tyr323 phosphorylation, p38α is autoactivated and monophosphorylated on Thr180. (b) A ribbon cartoon of wild-type p38α (PDB code 1P38). As for other kinases, the overall topology of p38 consists of N′- and C′-lobes forming the catalytic groove between them. The phosphorylation lip located between the lobes is colored gray. The L16 loop region, which is part of the C-terminal extension, and the adjacent C-helix are shown in red and blue, respectively. Tyr323, the alternative phosphoacceptor located in the L16 loop region, is shown in black and indicated by an arrow. The MKI, which is a signature feature of the family, is located at an external part of the C′-lobe consisting of two helices connected by a short loop (shown in orange). All molecular graphics figures were generated using PyMOL.[23]

render an intrinsically active enzyme. Since no amino acid can structurally mimic pTyr, we conducted a targeted and comprehensive search of the 323 activation site. Previous results of Tyr323 mutagenesis into Ser or Leu showed low intrinsic activity of less than 1% of activated $p38\alpha^{wt}$.[39] Additionally, Tyr323Phe in T-cells abolished p38α activation via the alternative pathway.[29]

Comprehensive and targeted site-directed mutagenesis of Tyr323 resulted in all but two mutants with intrinsic activity higher than the basal $p38\alpha^{wt}$ state. The five most active mutants and the least active Tyr323Phe mutant were chosen for further studies. The active mutants may emulate the conformational changes induced by Tyr323 phosphorylation and thus reveal structural features responsible for the alternative activation mechanism of p38α in T-cells. The crystal structures of selected active and inactive mutants were determined to evaluate the corresponding structural changes. Dramatic conformational changes occurred in the mutated active molecules that provide unique insight into the factors promoting autoactivation. The active mutants $p38\alpha^{Y323Q}$, $p38\alpha^{Y323R}$, and $p38\alpha^{Y323T}$ show substantial changes in the kinase interlobe orientation while this orientation remains similar to that of the wild-type structure in the inactive mutant $p38\alpha^{Y323F}$. These mutant-induced changes are part of the DEF site interaction pocket and make the active site receptive for autophosphorylation, suggesting that similar conformations may be also induced by Tyr323 phosphorylation. The residue-323 active mutants may be a useful tool for understanding the alternative activation pathway exclusive to T-cells and the differences between MKK-dependent activation and ZAP-70 activation in these cells. This would be an important stage in understanding the versatile MAPK signaling pathways and their resulting phenotypes.

## Results

### Design, expression, and purification of $p38\alpha^{Y323}$ mutants

The crystal structures of the $p38\alpha^{F323L}$ and $p38\alpha^{F323S}$ mutants have shown local conformational changes in the L16 loop region.[41] Phosphorylation of the proximal Tyr323 of $p38\alpha^{wt}$, which is also part of L16, was hypothesized to induce a similar subset of conformations resulting in a similar activation mechanism. The ability to functionally emulate the effect of phosphorylated Tyr323 via mutagenesis was tested by constructing a set of 17 p38α mutants, each with a different residue at position 323. The two remaining mutants, $p38\alpha^{Y323L}$ and $p38\alpha^{Y323S}$, have been described and assayed previously.[39] The mutants were expressed in *Escherichia coli* as N-terminal hexahistidine-tagged proteins and purified by $Ni^{2+}$-CAM affinity chromatography. All mutants were expressed as soluble proteins in *E. coli*, except for $p38\alpha^{Y323P}$, which was insoluble and was thus not included in further assays.

### Biochemical analysis of the 323-site mutants

The purified mutant proteins were assayed for their ability to phosphorylate glutathione *S*-transferase-activating transcription factor (ATF) 2 *in vitro*. $p38\alpha^{wt}$ was used as a negative control while the activity of MKK6-activated, dually phosphorylated p38α was set to 100%. Activities were monitored quantitatively using paper-spotted assay and qualitatively by separating the reaction mixture on SDS-PAGE and examining the radiolabeled, phosphorylated substrate. Of the 16 $p38\alpha^{Y323}$ mutants examined, 5 mutants—$p38\alpha^{Y323A}$, $p38\alpha^{Y323D}$, $p38\alpha^{Y323Q}$, $p38\alpha^{Y323R}$, and $p38\alpha^{Y323T}$—displayed an intrinsic activity of 1–3% relative to the activity manifested by MKK6-activated $p38\alpha^{wt}$ (Fig. 2a and b). These activities are relatively low compared to those previously described for the intrinsically active mutants $p38\alpha^{D176A}$, $p38\alpha^{F327L}$, and $p38\alpha^{F327S}$, which had ~10% activity[40] but are comparable to that of Thr-monophosphorylated p38α.[42] Mutating Tyr323 to the two other aromatic residues, $p38\alpha^{Y323F}$ and $p38\alpha^{Y323W}$, resulted in proteins that displayed lower intrinsic activities than inactivated $p38\alpha^{wt}$ (Fig. 2a and b). The activity levels of most Tyr323 mutants after activation by $MKK6^{EE}$ were comparable to those of $p38\alpha^{wt}$, while phosphorylated $p38\alpha^{Y323F}$ exhibited 76% of the level of activity of phosphorylated $p38\alpha^{wt}$ (Fig. 2c).

In order to evaluate whether the intrinsic activity of the p38α Tyr323 mutants is a result of phosphorylation, we monitored their phosphorylation status via a Western blot assay using anti-p-p38. Figure 2d shows that the active Tyr323 mutants have higher phosphorylation levels than $p38\alpha^{wt}$, whereas the inactive $p38\alpha^{Y323F}$ mutant is not phosphorylated (Fig. 2d). The levels of phospho-Thr and phospho-Tyr were evaluated separately using anti-pTyr and anti-pThr antibodies, but these assays resulted in very weak signals, probably indicating low specificities.

A "kinase-dead" version of the active variant $p38\alpha^{Y323Q}$ was constructed and expressed to determine if the spontaneous phosphorylation of the expressed mutants is a result of autophosphorylation. Western blot analysis clearly indicated that the $p38\alpha^{Y323Q+K53A}$ mutant is not phosphorylated (Fig. 2e), strongly suggesting that $p38\alpha^{Y323Q}$ is autophosphorylated and that the other active mutants become active via a similar mode of activation.

### The structures of $p38\alpha^{Y323}$ mutants

The structural changes that occur upon mutating Tyr323 were determined by comparing the X-ray

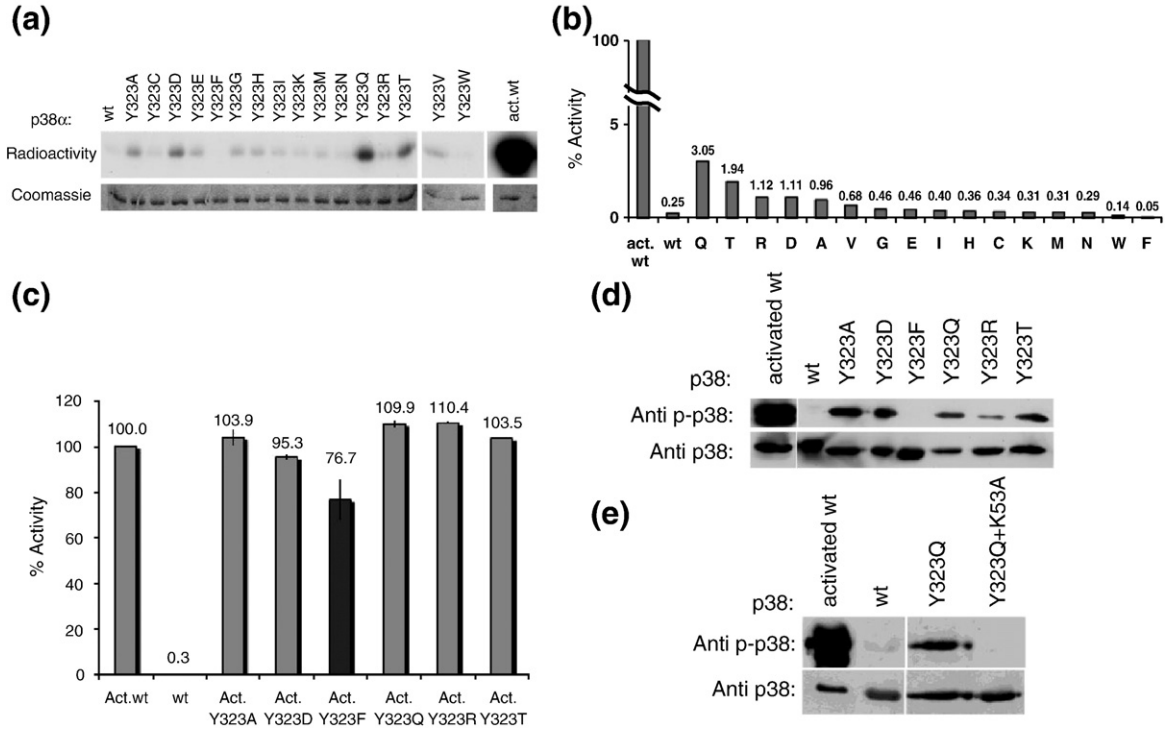


**Fig. 2.** *In vitro* catalytic activity and phosphorylation status of p38α molecules mutated at position Tyr323. (a) All the p38α$^{Y323}$ mutants and p38α$^{wt}$, purified from *E. coli*, were subjected to a kinase assay using glutathione *S*-transferase-ATF2 as a substrate, without additional activation. The MKK6$^{EE}$-activated p38α$^{wt}$ was used as a positive control. At the end of each reaction, a fixed volume was loaded on a gel. Equal amounts of substrate were present in each reaction as verified by the Coomassie staining (lower image). Radioactivity was monitored by exposing the gel to X-ray film (upper image). Note that some of the Tyr323 mutants show intrinsic activity independent of MKK activation. (b) Using the paper-spotted kinase assay technique, we quantified the activities of the mutants. The activity of the MKK6$^{EE}$-activated p38α$^{wt}$ was defined as 100%. The plot displays the average of three independent experiments with a standard error <15%. Of the 16 p38α$^{Y323}$ mutants assayed, 5 (p38α$^{Y323A}$, p38α$^{Y323D}$, p38α$^{Y323Q}$, p38α$^{Y323R}$, and p38α$^{Y323T}$) displayed intrinsic activity of 1–3% in comparison to that of the MKK6-activated p38α$^{wt}$. The two aromatic 323-mutated mutants (p38α$^{Y323F}$ and p38α$^{Y323W}$) exhibited lower activity than the inactive p38α$^{wt}$. (c) The ability of the active mutants to be activated by MKK6$^{EE}$ was determined using the paper-spotted kinase assay. All the Tyr323 mutation active mutants maintained their inherent ability to be activated by MKK6$^{EE}$ to an extent comparable to that of the wild type. Conversely, the MKK6$^{EE}$-activated p38α$^{Y323F}$ mutant displayed a lower activity of 76%. Two independent assays were conducted (in triplicate), and the average results are given. (d) Active mutants are spontaneously autophosphorylated. Western blot analysis using the anti-p-p38 antibody of p38α$^{Y323}$ mutants showing their autophosphorylation levels in comparison to the MKK6$^{EE}$-activated p38α$^{wt}$. Samples of the five active mutants and the inactive p38α$^{Y323F}$ were assayed. The active mutants were autophosphorylated in *E. coli*, whereas the inactive mutant displayed no phosphorylation (upper panel). Anti-p38 verified the amount of protein assayed (lower panel). (e) Western blot analysis of the p38α$^{Y323Q+K53A}$ mutant compared to p38α$^{Y323Q}$ and p38α$^{wt}$. The K53A kinase-dead mutant abolishes the phosphorylation level of p38α$^{Y323Q}$, indicating that activation of the intrinsically active mutants results from their autophosphorylation capabilities.

structures of p38α$^{Y323Q}$, p38α$^{Y323T}$, and p38α$^{Y323R}$ variants that exhibited intrinsic activity and p38α$^{Y323F}$, whose activity was shown to be lower than that of p38α$^{wt}$ (Fig. 2b). The crystallization profile of active p38 mutants was significantly different from those of the wild type and inactive mutant, which implied structural differences. The crystal structure of the p38α$^{Y323F}$ mutant was highly similar to that of p38α$^{wt}$ in most features. Minor differences between the structures were mainly in the vicinity of the mutation site. In p38α$^{wt}$, Tyr323 was located in a hydrophobic pocket that accommodated its ring and was mostly unavailable to solvent. The hydroxyl of Tyr323 formed a polar interaction with C-helix Arg70 main-chain carbonyl oxygen bridged by a water molecule (Supplemental Fig. 2). Tyr323 can also be considered part of the extended hydrophobic core defined by Tyr69, Phe327, and Trp337.[39,40] Consequently, the lack of the hydroxyl group in the Tyr-to-Phe mutation resulted in a 1.1-Å shift of the residue toward Phe327 and a main-chain shift of 1–1.2 Å in residues 327 to 333, inducing a slight conformational change in the backbone of this region (Fig. 3a).

In contrast to the relatively minor changes induced by the Tyr323Phe mutation, the Tyr323Arg,

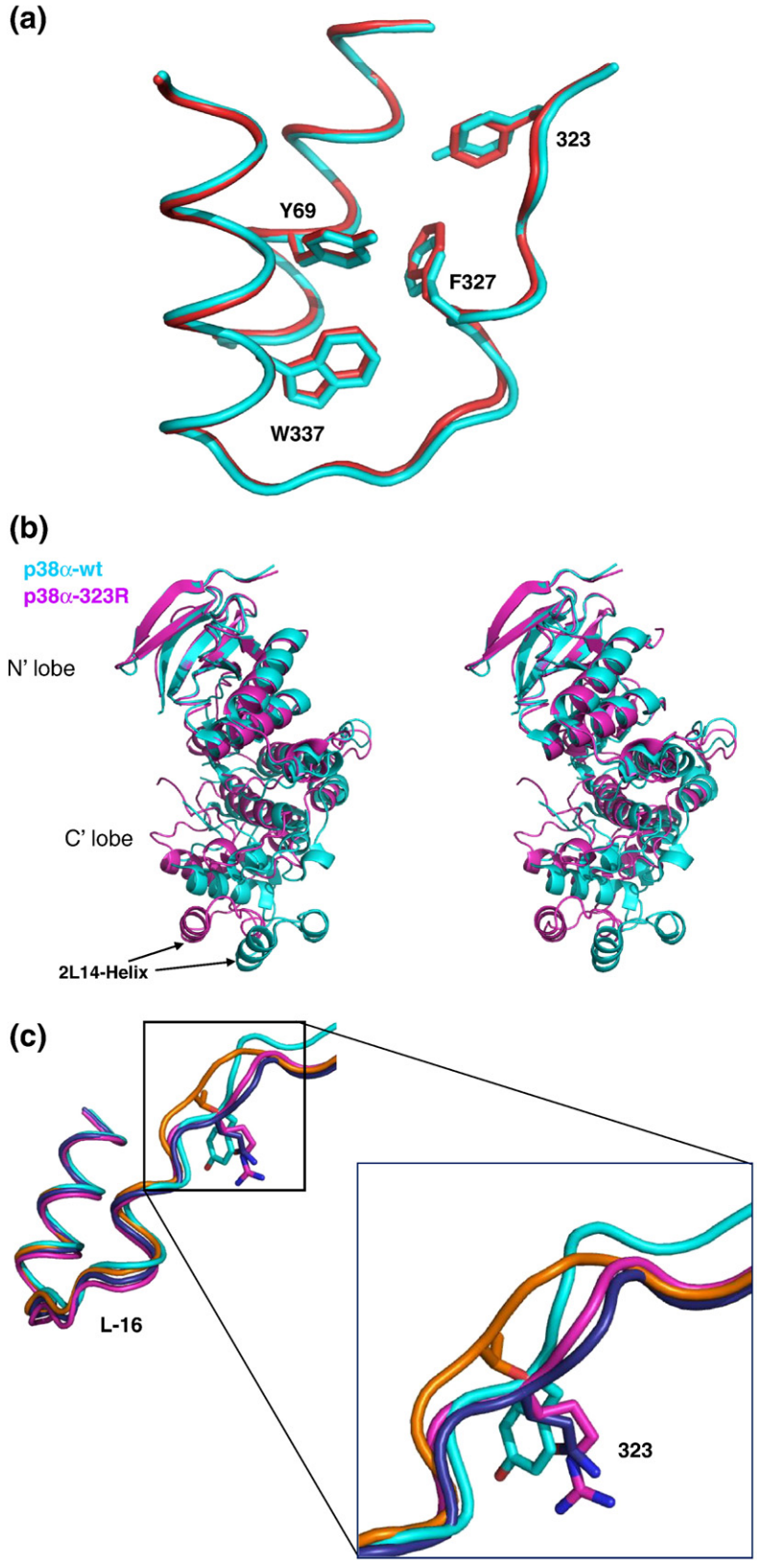


**Fig. 3** (*legend on next page*)

Tyr323Thr, or Tyr323Gln mutant displayed remarkable conformational changes in the kinase interlobe orientation ( Fig. 3b and Supplemental Fig. 3). The overall changes observed in the structures of active mutants do not result from crystal packing considerations since most of the altered regions do not form crystal contacts. The MKI region at the C′-lobe showed a 12-Å shift relative to the wild-type protein when the N′-lobes were superimposed (Fig. 3b). More specifically, the 323-mutated residues oriented differently from Tyr323 in the wild-type model. These residues were rotated outwards from the wild-type Tyr orientation, and their polar nature prevented them from being accommodated in their previous positions. The changes were also reflected in L16, which shifted together with its adjacent interlobe linker (residues 305–320) (Fig. 3c). In general, the newly positioned 323-residue did not permit the same interlobe orientation observed for the wild-type protein, mainly due to steric clashes, and thus induced a distinctly different local fold with a new orientation.

Although all three active mutants showed a similar interlobe shift, each of them induced a somewhat different change. They can be roughly divided into two subgroups based on the size of their side chains and corresponding interlobe shift. The side chains of Gln and Arg are larger than that of Thr, which was reflected in the resultant interlobe orientation. The larger side chains of Gln or Arg at position 323 induced one subtype of lobe displacement, whereas the smaller Tyr323Thr mutation induced a somewhat different type. A short segment in L16 near the mutation site (residues 320–324) also differs between the two subgroups (Fig. 3c).

In p38α$^{wt}$, there are several interactions between the L16 loop region and the C-lobe that stabilize the interlobe orientation. Gln325 forms a polar H-

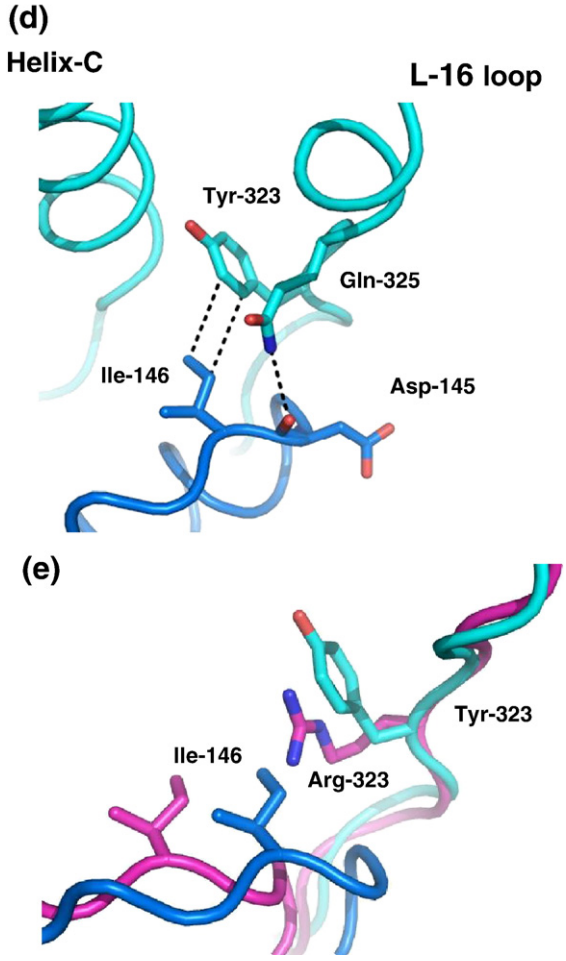


**Fig. 3.** Conformational changes of p38α position-323 mutants. (a) Tube representations of superimposed p38α$^{Y323F}$ (red) and p38α$^{wt}$ (cyan) showing the hydrophobic core of the kinase N′-lobe defined by aromatic residues in L16 and the C-helix. L16, a molecular switch that induces autoactivation and undergoes conformational changes upon activation, is stabilized by hydrophobic core interactions. In the wild-type structure, Tyr323 is located in a hydrophobic pocket that accommodates its ring. The missing hydroxyl group in the Tyr-to-Phe mutation results in a shorter distance between the two side chains of Phe327 and Phe323 (from 5 Å to 3.8 Å), thus increasing the stability of the hydrophobic core. (b) Stereo presentation of the superimposed p38α$^{wt}$ (cyan) and p38α$^{Y323R}$ (magenta). The N′-lobes of the models were superimposed, emphasizing the substantial differences in the C′-lobe position. Short arrows and a label indicate the positions of the 2L14 -helix from the MKI shifting 12 Å in the mutation (measured from Gln253 C$^{\alpha}$). The p38α$^{Y323R}$ model is representative of all other active mutants, which are shown in Supplemental Fig. 3. (c) Local conformational changes in the L16 loop region near the mutation site. All models were superimposed on the proximal C-helix in the N′-lobe showing p38α$^{wt}$ (cyan), p38α$^{Y323R}$ (magenta), p38α$^{Y323Q}$ (blue), and p38α$^{Y323T}$ (orange). The displayed segment spans from residue 319 to 346, highlighting the changes in the main-chain conformation and the side-chain position. On the right is an enlargement of the segment including the mutation site. The 323-mutated residues of the active mutants are rotated outwards form the wild-type Tyr position. Note the unique position of the Thr323 mutant compared to Gln323 and Arg323, which form two distinct subpopulations and are also reflected in other structural features. (d) Part of the interlobe interface of p38α in the vicinity of Tyr323 includes H-bonding between the Gln325 N$^{\varepsilon 2}$ from the N′-lobe and the main-chain carbonyl oxygen of Asp145 from the C′-lobe. The aromatic ring side chain of Tyr323 also forms hydrophobic interactions with Ile146. For clarity, the N′-lobe and C′-lobe segments are colored cyan and light blue, respectively. (e) Superposition of the wild type (cyan) and Tyr323Arg mutation (magenta) on the L16 loop. Due to the consequent conformational changes, the wild-type interactions [shown in (d)] could not be maintained due to steric clashes. Arg323 is too close to the wild-type position of Ile146, and the corresponding loop with the C′-lobe is shifted to its new position. The polar interaction between Gln325 and Asp145 [shown in (d)] could not be formed in the mutant state.

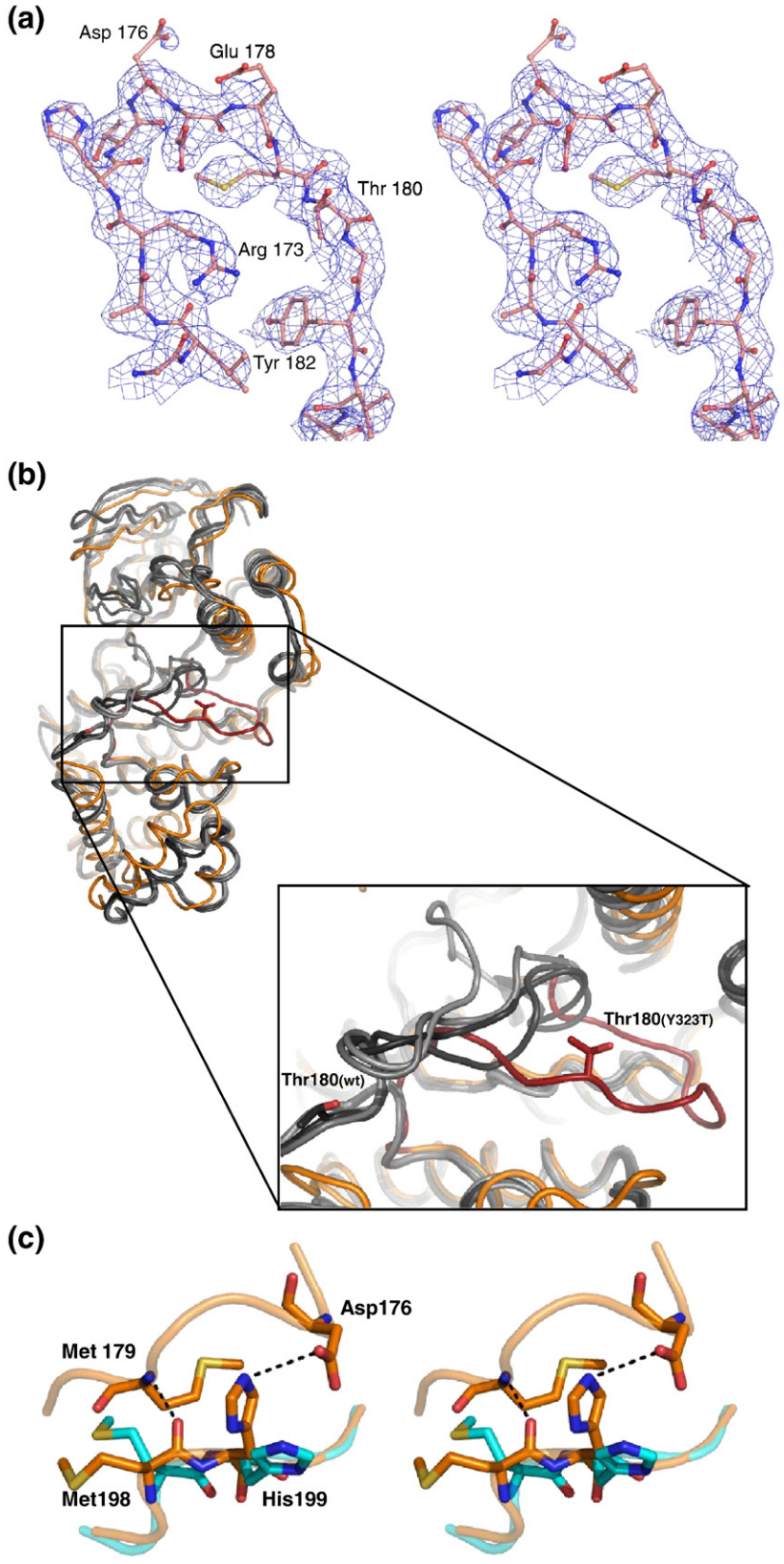


**Fig. 4.** The phosphorylation lip of the Tyr323Thr mutant adopts a novel and extended conformation. (a) Stereo view of the final $2F_{obs} - F_{calc}$ electron density map of the Tyr323Thr mutant calculated for the resolution range of 50–2.7 Å at 1 σ cutoff, displaying the final phosphorylation lip of the final model. (b) Analysis of five representative, available p38 structures containing the loop in their models shows entirely different conformational populations (shown in gray; PDB codes 1A9U, 1OUK, 1P38, and 3KQ7). The orientation of the phosphorylation lip in p38α$^{Y323T}$ (shown in red) exhibits a unique conformation that was not observed earlier in any p38α model. The activation loop in the p38α$^{Y323T}$ mutant adopts a more extended and exposed conformation, making the Thr180 (labeled) more solvent accessible. This loop adopts a more compact conformation in the other models. (c) Stereo presentation of a short segment of the phosphorylation lip of Tyr323Thr mutant (orange) interacting with the αEF/αF loop in comparison to the wild-type model (cyan). The phosphorylation lip conformation and the accompanying conformational change of the αEF/αF loop form stabilizing polar interactions. Two polar interactions are formed between the main-chain carbonyl oxygen of Met198 and the main-chain amide nitrogen of Met179 and between His199 $N^{\varepsilon 1}$ and Asp176 $O^{\delta}$.

bond with Asp145 located in the loop connecting the E-helix and β6 of the C′-lobe, residues 144–145. Additionally, Tyr323 forms a hydrophobic interaction with Ile146 (from β6 of the C′-lobe) (Fig. 3d). These interactions are prevented by steric clashes due to the conformational changes in the L16 loop region upon mutating Tyr323 to Gln or Arg (Fig. 3e). The shift in the interlobe orientation satisfies steric requirements of the interlobe interface (Fig. 3e).

The side chain of Thr323 in p38α$^{Y323T}$ is too small to induce the steric clashes described for the larger residues; thus, the observed conformational changes probably did not result solely from steric considerations. The structure of p38α$^{Y323T}$ exhibited some local changes in the segment of residues 320–324 (Fig. 3c). The distance between His77 $N^{\varepsilon 2}$ and Asp321 main-chain oxygen was too large (4.6 Å) to maintain the hydrogen bond found in the wild type and other position-323 active mutants, with an average distance of 2.8 Å (not shown). Since the L16 loop region is part of the segment connecting the lobes, the local change induced by Thr323 was reflected in different interlobe orientations compared to that of p38$^{wt}$.

### The phosphorylation lip

The availability of the phosphorylation lip (residues 171–183) also differs between the two 323 active mutant subgroups in the model. The phosphorylation lip region was not modeled in most of the available p38 structures due to its flexibility. The complete loop segment of all but one of the 323 active mutants could not be modeled since the electron density map in this region was weak and discontinuous. Only p38α$^{Y323T}$ had a clear and interpretable electron density map in this region and was modeled (Fig. 4a and b). However, the overall trace of the loop of the p38α$^{Y323R}$/p38α$^{Y323Q}$ mutants resembled that of p38α$^{Y323T}$ rather than that of available wild-type models. The differences in the stabilization of the activation loops of the 323 active mutants probably resulted from the corresponding interlobe orientations. The shift of the lobe in p38α$^{Y323T}$ was relatively larger than that in p38α$^{Y323Q}$ and p38α$^{Y323R}$. As a consequence, the new and more exposed loop orientation in p38α$^{Y323T}$ formed stabilizing interactions with the C-helix (residues 63–78), L16, and the short αEF/αF loop (residues 196–202), which followed the phosphorylation lip (Fig. 4c). The phosphorylation lip of p38α$^{Y323T}$ adopted a unique exposed conformation that has not previously been observed in any p38 structure in which the loop was modeled. In this conformation, the position of the Thr180 phosphoacceptor is substantially shifted by 17 Å (between $C^{\alpha}$ atoms) compared to the wild-type models (Fig. 4b).

### The DEF site interaction pocket

The DEF site interaction pocket is located in the C-lobe and comprises residues from several segments including the loop connecting P+1 and F-helix (residues 203–217), which precedes the activation loop, the G-helix (residues 227–237), the MKI region (residues 240–262), and part of the phosphorylation lip (residues 180–182)[36] (Fig. 5a). In the inactive p38α models, the DEF site interaction pocket is unavailable and thus unreceptive for substrate binding. The structures of the 323 active mutants displayed conformational changes in the C′-lobe, which enabled the formation of the DEF site interaction pocket. More specifically, in the p38α$^{Y323T}$ mutant, changes were observed in the phosphorylation lip where the $C^{\alpha}$ atoms of the TGY motifs are shifted by more than 17 Å to form the DEF site rim close to the p38 active site (Fig. 5b). In addition, notable shifts are also observed in other residues contributing to the DEF site interaction pocket. In this regard, Leu195 and Trp197 move by more than 5 Å ($C^{\alpha}$ distances) to form the pocket where other contributing residues are shifted by distances between 1 and 3.5 Å (Fig. 5a and b). This formed a pocket with a hydrophobic cavity similar to that observed for the dually phosphorylated ERK2[37] (Fig. 5c). In the p38α$^{Y323Q}$ and p38α$^{Y323R}$ active mutants, the changes and corresponding shifts in the C-lobe that form the DEF site interaction pocket were similar to those observed for the p38α$^{Y323T}$ mutant (not shown). The general pocket-like shape of the DEF site lacked the rim formed by the C-lobe due to the lack of the phosphorylation lip in the model.

## Discussion

The canonic, well-characterized MAPK pathway is one of the critical signaling cascades in all eukaryotic cells and is involved in most vital cellular processes. MAPK activation requires dual phosphorylation on neighboring Thr and Tyr residues. This mode of activation is unique among kinases that commonly require monophosphorylation of Thr for activation.[43] Most kinases are phosphorylated and activated via autophosphorylation.[43,44] Recent findings, primarily with p38, have suggested that MAPKs can also be activated via autophosphorylation. The p38α alternative activation pathways in T-cells may provide at least a partial explanation for the features promoting autoactivation. This study focused on the structural changes that occur upon mutating the alternative phosphorylation site Tyr323. The resulting structures displayed remarkable details of the unique conformational changes that induce autoactivation of p38α and revealed the molecular basis of their

activity. Some of the mutants rendered the molecule intrinsically active at relatively low levels (1–3%) compared to the dually phosphorylated form (normalized to 100%). These levels of activity are comparable to those of Thr180-monophosphorylated p38α.[42,45] Interestingly, Tyr323 phosphorylation leads to autoactivation in trans of p38 and subsequent monophosphorylation of the activation loop Thr180.[28]

The X-ray structures of the mutants showed that the change from Tyr323 to Phe induced Phe327 and Phe323 to form hydrophobic interactions that increased the stability of the hydrophobic core. The L16 loop region has been postulated to undergo conformational changes upon activation, and this has been observed in ERK2 structures. In addition, we have previously shown that the L16 loop region of p38α can be regarded as a molecular switch that

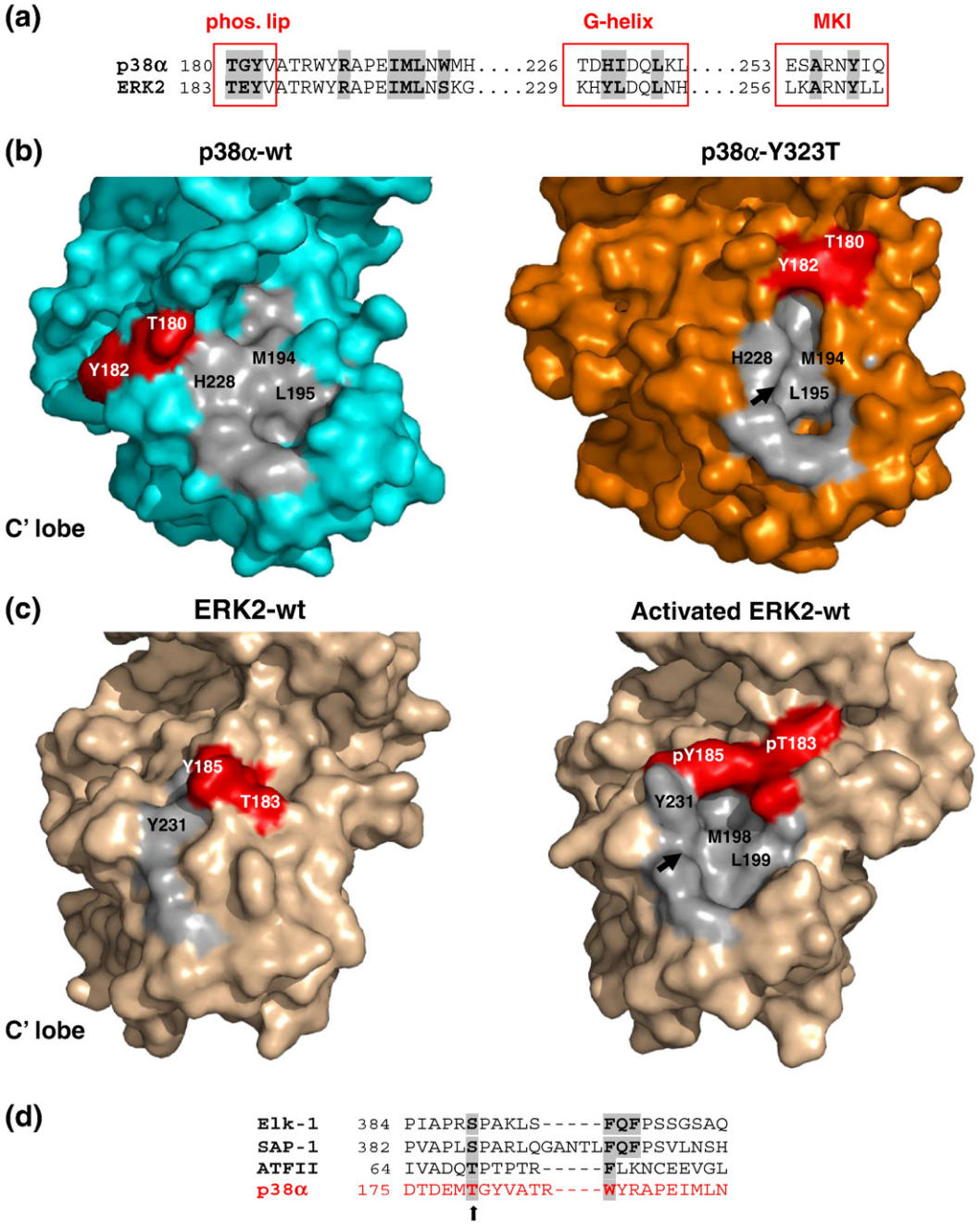


**Fig. 5** (*legend on next page*)

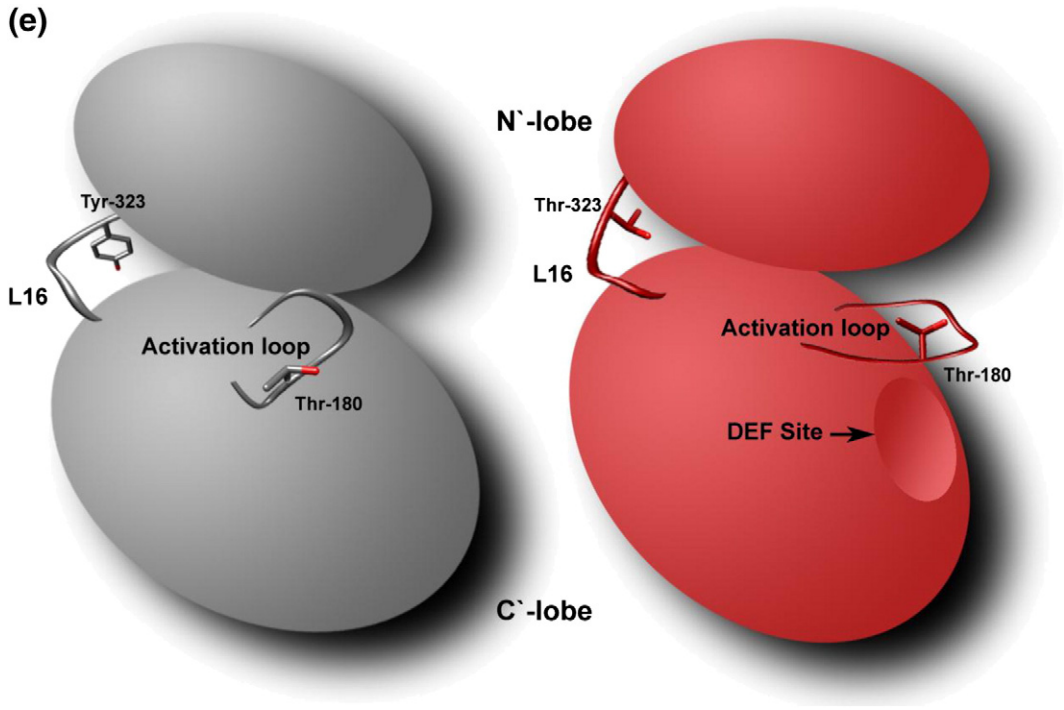


**Fig. 5.** The DEF site interaction pocket in p38α and ERK2. (a) The segments defining the DEF site interaction pocket (highlighted in gray) indicated in the sequence alignment of p38α and ERK2. The individual residues that participate in the DEF site pocket are highlighted in gray and show a high level of similarity between the two proteins. In p38α and ERK2, the pocket is defined by selected hydrophobic residues that came from the phosphorylation lip, a loop that follows the phosphorylation lip, the G-helix, and the MKI region. (b) Surface presentation of $p38\alpha^{wt}$ (cyan, left; adopted from the 1P38 model) and $p38\alpha^{Y323T}$ (orange, right) highlighting the residues forming the DEF site interaction pocket. The residues contributing to the pocket are highlighted in gray, and TGY from the phosphorylation lip are in red. For clarity, only the C′-lobe of the molecular surface is displayed. Tyr323Thr mutation forms the DEF site interaction pocket, which can accommodate hydrophobic residues to stabilize its substrate. In the $p38\alpha^{Y323R}$ and $p38\alpha^{Y323Q}$ mutants, the phosphorylation loop was not modeled, yet the cavity indicating the DEF site interaction pocket is also formed. Labels indicate the positions of selected residues contributing to the DEF site. (c) The formation of the DEF site interaction pocket was initially observed upon conformational changes consequent to activation of ERK2. The inactive form (left) and the dually phosphorylated form (right) indicate the formation of the hydrophobic pocket. The residues contributing to the pocket and the TEY phosphoacceptors are colored gray and red, respectively. Selected residues contributing to the DEF site are indicated by labels. (d) Sequence alignment of the segments including the Thr phosphoacceptor in p38α and three selected substrates (ATF2, SAP1, and Elk1). A gap of 6–12 residues between the Thr phosphoacceptor and an aromatic side chain that could be accommodated in the DEF site interaction pocket is shown, although larger gaps are also allowed. (e) Cartoon of the conformational changes induced in the Tyr323 active mutants (pink, right) compared to $p38\alpha^{wt}$ (gray, left). The active mutants induce substantial changes in the kinase interlobe orientation, which, together with the unique and extended conformation of the activation loop, contribute to the formation of the additional substrate DEF site interaction pocket. These changes may confer an appropriate conformation for autophosphorylation in trans as for pTyr323 in p38α.

upon conformational changes induces auto-activation.[46] The increased stability of the hydrophobic core presumably hinders the required conformational changes upon activation in this region, which consequently results in lower activity. The increased stability of the L16 hydrophobic core was also reflected in the lower activity (76%) of the dually phosphorylated form of $p38\alpha^{Y323F}$ (Fig. 2c).

Unlike $p38\alpha^{Y323F}$, the structures of intrinsically active mutants $p38\alpha^{Y323Q}$, $p38\alpha^{Y323R}$, and $p38\alpha^{Y323T}$ displayed dramatic conformational changes that may indicate factors promoting their activities. Despite differences in their chemical nature, their induced molecular structural changes are similar. The most notable change is the unique interlobe orientation, probably making the kinase active site more substrate receptive. Our initial assumption was that phospho-Tyr323 induces local conformational changes similar to those observed for L16 in the $p38\alpha^{F327L}$ and $p38\alpha^{F327S}$ active mutants, suggesting a similar mechanism.[46] However, the 323 active mutants displayed substantially different changes, both locally (L16 loop) and globally, probably indicating a different activation mechanism. It could be thus suggested that Tyr323 restrains L16 in a conformation, maintaining the low basal activity

of p38α by preventing autophosphorylation. Such extreme structural changes have been observed for phosphorylated MAPKs. Only two structures, ERK2 and p38γ, have dually phosphorylated forms where only ERK2 is available in both the inactive and the active modes.[37,47] Upon phosphorylation, the two phosphoacceptors in ERK2 and p38γ form a network of polar interactions, resulting in a new interlobe orientation that induces a conformational change of the activation loop and consequently exposes the MAPK active site to substrates.

The conformation of the activation loop in p38α$^{Y323T}$ may provide another clue to its intrinsic activity. In most p38α structures, the activation loop has no defined conformation. In p38α models where the loop is defined, all conformations differ substantially from those observed in the p38α$^{Y323T}$ mutant described here (Fig. 4b). The conformation of the p38α$^{Y323T}$ activation loop displayed higher availability and accessibility of the p38α active site, which may account for its intrinsic activity. Similar conformational changes in L16 and resulting exposed activation loop have also been observed in the structures of ERK2 complexed with short docking-site binding peptides. Upon peptide binding, conformational changes occur in the L16 region, near the common docking motif, resulting in an extended conformation of the activation loop that differs from both phosphorylated and non-phosphorylated forms.[48]

In p38α$^{Y323T}$, the unique conformation of the phosphorylation lip also contributed to the DEF site interaction pocket, which has been identified as an additional docking site in MAPKs.[32,36] This site was initially identified in ERK2 and is formed as part of the conformational changes occurring upon activation.[37] This distinctive docking motif is assumed to accommodate large hydrophobic or aromatic side chains 6–20 residues downstream to the phosphoacceptor with high selectivity toward transcription factors.[49–52] It has been recently shown, using substrate-derived peptides, that p38α and p38β also contain a DEF site interaction pocket.[36] Additionally, mutagenesis of SAP-1 transcription factor on the DEF site binding region unequivocally verifies its significance for efficient phosphorylation by p38α[35] (Fig. 5a).

Structural analysis of the active mutants provided the first substantiation for the formation of the DEF interaction site in p38α. In the 323 active mutants, the DEF site interaction pocket, formed by changes in the C′-lobe, could promote autophosphorylation by accommodating part of the now extended and available phosphorylation lip of another p38α molecule. The sequence of the phosphorylation lip of p38α includes aromatic side chains (Trp187 and Tyr188) seven and eight residues away from the Thr180 phosphoacceptor (Fig. 5a). These aromatic residues from the lip may be anchored in the DEF site pocket where, consequently, Thr180 becomes embedded in the active site near the catalytic residues and consequently phosphorylated, rendering the molecule active.

It has been repeatedly shown that Asp and Glu can at least partially functionally replace the phosphorylated state of Ser and Thr.[53,54] However, there are no standard amino acids that are structurally and chemically similar to phospho-Tyr. We were able to functionally emulate pTyr323 in p38α by imposing conformational changes that promote autoactivation. The combined features of the interlobe orientation, active-site components, phosphorylation lip conformation, and formation of the DEF site interaction pocket all provided a groundbreaking view into the unique activation state of p38α that is probably attained upon Tyr323 phosphorylation and leads to auto-monophosphorylation of Thr180 (Fig. 5e). Differences between the monophosphorylated and the dually phosphorylated forms presumably dictate substrate selectivity, resulting in different cellular phenotypes. These mutants are unique candidates for studying p38 activation in T-cells as well as in other cell systems.

## Materials and Methods

### Site-directed mutagenesis of the p38α mutants

Site-directed mutagenesis of the p38α$^{Y323}$ site was carried out using a QuickChange kit (Stratagene). Mutagenesis was performed on the human p38α$^{wt}$ cDNA subcloned into pET-28a (Novagen) vector downstream and in-frame with the hexahistidine coding sequence. The procedure included polymerase chain reaction using specific complementary primers (Supplemental Table 1). Mutagenesis of the p38α$^{Y323Q+K53A}$ was performed on the pET-28a vector containing p38α$^{Y323Q}$ as a template using specific complementary primers (Supplemental Table 1). All mutated cDNAs were verified by sequencing of the entire p38α cDNA.

### Paper-spotted kinase assay and Western blot

Cell cultures (0.5 L) were grown at 30–32 °C in order to obtain phosphorylated and active mutants. Protein expression and purification, as the *in vitro* kinase assay, were conducted in triplicate as previously described.[40] In parallel, for a quality assay, samples from the paper-spotted kinase reactions were mixed by applying Laemmli sample buffer and boiling at 100 °C for 5 min. The assay samples were run on SDS-PAGE, stained with Coomassie staining, and then exposed to X-ray film for ~6 h with intensifier.

For the Western blot assay, 0.3 μg of purified recombinant protein was heated at 100 °C for 5–10 min, separated by SDS-PAGE, and then transferred to a nitrocellulose membrane. After incubating the membrane with the appropriate antibodies, we visualized specific proteins

using an enhanced chemiluminescence detection reagent and then monitored them by exposing membranes to X-ray film and by densitometry. Goat anti-p38 was obtained from Santa Cruz Biotechnology and rabbit anti-phospho-p38 was obtained from Cell Signaling.

### Crystallization of p38α mutants

For crystallization purposes, cell cultures (3–6 L) were grown at 21 °C, resulting in homogeneous non-phosphorylated protein as previously described.[46] Expression at higher temperatures (30–32 °C) yielded an increased amount of (heterogeneously phosphorylated) protein, which was unsuitable for crystallization assays as occurred previously for other p38α active mutants.[41,46] Expression and purification protocols for crystallization purposes were conducted as previously described.[46] The position-323 mutants were crystallized by applying conditions similar to those obtained for p38α$^{wt}$.[41,46] Subsequently, as previously described, the streak-seeding method was employed to induce crystallization using wild-type crystals as the source of microseeds.[55] Crystals for all mutants were obtained using the vapor diffusion sitting-drop method at 4 °C with a 6-μL crystallization droplet containing equal amounts of protein and reservoir solution. Crystallization assays of the p38α$^{Y323F}$ inactive mutant were conducted using 1 ml reservoir solution containing 17% (w/v) polyethylene glycol 3350, 0.1 M Hepes (pH 7.25), 0.2 M potassium fluoride, and 25 mM *n*-octyl-β-D-glucopyranoside (β-OG). After 4 h of equilibration at 4 °C, streak seeding was applied using p38α$^{wt}$ crystals to initiate crystallization. Two to three days after seeding, crystals appeared with morphology similar to that of p38α$^{wt}$; however, they exhibited relatively poor diffraction. An additive screen was employed, and diffraction improved after adding 20 mM $AlCl_3$ to the reservoir solution.

The active mutants were crystallized using conditions similar to that of the p38α$^{Y323F}$ mutant and its crystals as a source of microseeds. Two to three days after seeding, massive precipitation appeared with no apparent crystals. Clusters of spherical needle-like clusters appeared after 8–10 days, indicating that p38α$^{Y323}$ active mutants exhibit a different crystallization profile (conditions, morphology) compared to the previously obtained ones. When the mutant was crystallized without seeding, similar crystals appeared spontaneously after a week. After changing the crystallization conditions (pH from 7.25 to 7.75, potassium fluoride from 0.2 M to 0.1 M, and polyethylene glycol 3350 from 15% to 19%), we obtained clusters of very thin needle-like crystals. With the use of these crystals for streak seeding, clusters of very thin and small plate-like crystals appeared. After some additional seeding cycles, individual thin-plate crystals were obtained. The first active mutant to be crystallized with this morphology was p38α$^{Y323R}$, and its crystals were used for further cross seeding to obtain crystals of p38α$^{Y323Q}$ and p38α$^{Y323T}$ active mutants that exhibited similar external morphology. Prior to data collection, the crystals of the p38α$^{Y323F}$

**Table 1.** Data collection and refinement statistics

| | p38α$^{Y323F}$ | p38α$^{Y323R}$ | p38α$^{Y323T}$ | p38α$^{Y323Q}$ |
|---|---|---|---|---|
| ESRF beamline | ID23-1 | ID29 | ID29 | ID29 |
| Wavelength (Å) | 0.9300 | 0.9300 | 0.9300 | 0.9300 |
| Space group | $P2_12_12_1$ | $P2_1$ | $P2_1$ | $P2_1$ |
| Unit cell parameters | | | | |
| *a*, *b*, *c* Unit cell parameters (Å) | 64.7, 69.0, 74.4 | 40.0, 72.3, 68.9 | 40.3, 71.7, 70.9 | 37.9 71.8 63.5 |
| β (°) | | 105.0 | 90.3 | 95.2 |
| Resolution range (Å) (last resolution shell) | 50–1.6 (1.66–1.6) | 50–2.3 (2.34–2.30) | 50–2.7 (2.75–2.70) | 50–2.2 (2.24–2.2) |
| Unique reflections | 44,779 | 17,020 | 11,276 | 15,566 |
| Reflections used in refinement | 44,655 | 15,850 | 10,735 | 14,808 |
| Redundancy | 7.7 | 3.6 | 3.1 | 3.3 |
| $R_{sym}(I)$[a] | 4.3 (75.8) | 9.4 (80.6) | 8.4 (56.6) | 7.2 (59.7) |
| Completeness | 99.9 (99.4) | 97.3 (96.9) | 99.0 (99.5) | 98.2 (95.7) |
| $I/\sigma$ | 29.0 (1.3) | 21.2 (2.3) | 16.3 (1.8) | 22.4 (2.6) |
| Number of protein atoms | 2714 | 2709 | 2781 | 2604 |
| Number of β-OG atoms | 40 | 40 | 20 | 20 |
| Number of solvent atoms | 329 | 23 | 22 | 12 |
| $R_{cryst}$ | 0.183 | 0.214 | 0.200 | 0.222 |
| $R_{free}$[b] | 0.221 | 0.281 | 0.283 | 0.304 |
| Average *B*-factor (Å$^2$) | | | | |
| Protein | 25.5 | 60.9 | 60.3 | 55.8 |
| β-OG | 27.9 | 66.0 | 57.8 | 66.8 |
| Solvent | 38.6 | 52.8 | 40.8 | 41.9 |
| rmsd from ideality | | | | |
| Bond length (Å) | 0.011 | 0.013 | 0.015 | 0.012 |
| Bond angle (°) | 1.37 | 1.66 | 1.66 | 1.43 |
| Ramachandran plot (%) (PROCHECK) | | | | |
| Favored | 90.7 | 86.4 | 85.6 | 84.0 |
| Allowed | 9.0 | 13.3 | 14.1 | 15.3 |
| Generously allowed | 0.3 | 0.3 | 0.3 | 0.7 |
| Disallowed | 0.0 | 0.0 | 0.0 | 0.0 |

[a] $R_{sym}(I) = \sum | I - \langle I \rangle | / \sum I$.
[b] Test set consists of 5% for all data.

mutant were cryo-protected using Paratone-N oil and immediately flash cooled in liquid nitrogen. The p38α$^{Y323Q}$, p38α$^{Y323R}$, and p38α$^{Y323T}$ crystals were cryo-protected using the corresponding reservoir solution with 20% glycerol.

### Crystallographic data collection and refinement

Crystallographic data for all p38α$^{Y323}$ mutants were collected at the European Synchrotron Radiation Facility (ESRF) (see Table 1). Data were integrated and scaled using the HKL suite.[56] The crystals of the p38α$^{Y323F}$ belonged to the orthorhombic $P2_12_12_1$ space group, and the crystals of the p38α$^{Y323Q}$, p38α$^{Y323R}$, and p38α$^{Y323T}$ mutants belonged to the monoclinic $P2_1$ space group, with one p38α molecule in the asymmetric unit for both symmetries (Table 1). The active p38 mutants exhibited some differences in their corresponding cell parameters (Table 1). Most of the thin-plate crystals of the active mutants displayed poor diffraction, and better-diffracting crystals could be identified only via extensive screening after which complete data sets were collected. The structure of the p38α$^{Y323F}$ mutant was solved via molecular replacement methods using Molrep[57] implemented in CCP4i using p38α [Protein Data Bank (PDB) code 2FSO[46]] as the search model after removing all solvent and detergent molecules. The solution resulted in an $R$ value of 0.46 and a score of 0.56 in the resolution range of 50–4.0 Å. The initial $F_{obs} - F_{calc}$ and $2F_{obs} - F_{calc}$ electron density maps were calculated after 10 cycles of restrained refinement using REFMAC5.[58] The structure was further refined in the resolution range of 50–1.6 Å using PHENIX,[59] and solvent molecules were added utilizing ARP/wARP.[60] The structure was fitted into electron density maps using the graphics program Coot.[61] The final p38α$^{Y323F}$ model ($R_{cryst}$ = 19.7; $R_{free}$ = 24.6) consists of residues 5–175, 185–263, and 267–352, with 380 solvent molecules and 2 β-OG molecules (Table 1).

The structure of the p38α$^{Y323R}$ mutant was solved via molecular replacement methods using Molrep with the structure of p38α$^{Y323F}$ as the search model. The solution resulted in an $R_{cryst}$ of 0.48 and a score of 0.42 in the resolution range of 66–4.0 Å. The solved structure was then refined by REFMAC5[58] using the rigid-body protocol defining the two kinase lobes as different domains (domain 1 included residues 5–110 and 320–352; domain 2 included residues 111–319) at the resolution range of 50–4.0 Å. $R_{cryst}$ was reduced from 47.2% to 44.1% after 20 cycles of refinement. Consequently, the model was refined using the REFMAC restrained refinement option in the resolution range of 50.0–2.3 Å, and $R_{cryst}$ decreased from 44.1% to 30.0%. The structure was further refined using PHENIX,[59] and solvent molecules were added utilizing ARP/wARP. The structure was fitted into electron density maps using the graphics program Coot. The p38α$^{Y323R}$ model consists of residues 4–31, 37–172, and 183–353, with 24 solvent molecules and 2 β-OG molecules (Table 1). The structures of the p38α$^{Y323Q}$ and p38α$^{Y323T}$ mutants were solved via molecular replacement methods using model p38α$^{Y323R}$ as a search model and refined by a similar protocol described above. For all 323 mutant structures, the initial electron density maps clearly indicated the presence of the mutated residue and their conformation (not shown). The p38α$^{Y323T}$ model was refined in the resolution limits of 50–2.7 Å using PHENIX[59] to a final $R_{cryst}$ of 20.0% ($R_{free}$ = 28.3%) and consists of residues 4–31 and 37–352, with 24 solvent molecules and 1 β-OG molecule (Table 1). The p38α$^{Y323Q}$ model was refined in the resolution limits of 50.0–2.2 Å to a final $R_{cryst}$ of 22.2% ($R_{free}$ = 30.4%) consisting of residues 4–31, 37–172, 183–242, and 257–353, with 14 solvent molecules and 1 β-OG molecule (Table 1).

### PDB accession codes

PDB coordinates and structure factors have been deposited with accession codes 3OD6, 3ODY, 3ODZ, and 3OEF for the Y323T, Y323Q, Y323R, and Y323F mutants, respectively.

## Acknowledgements

This research was supported by the Israel Science Foundation grant 630/07 and Israel Science Foundation Research Center of Excellence 180/09 awarded to O.L. and D.E. We would like to thank Dr. Mario Lebendiker from the Protein Purification Unit of the Wolfson Centre for Applied Structural Biology for his continuous helpful advice and assistance and to Dr. Deborah E. Shalev for help in constructing Fig. 5e and for insightful discussions. We would like to thank the staff of ESRF (Grenoble, France) for their outstanding help and for maintaining and upgrading the facility.

## Supplementary Data

Supplementary data to this article can be found online at doi:10.1016/j.jmb.2010.11.023

## References

1. Widmann, C., Gibson, S., Jarpe, M. B. & Johnson, G. L. (1999). Mitogen-activated protein kinase: conservation of a three-kinase module from yeast to human. *Physiol. Rev.* **79**, 143–180.
2. Jiang, Y., Gram, H., Zhao, M., New, L., Gu, J., Feng, L. *et al.* (1997). Characterization of the structure and function of the fourth member of p38 group mitogen-activated protein kinases, p38delta. *J. Biol. Chem.* **272**, 30122–30128.
3. Enslen, H., Brancho, D. M. & Davis, R. J. (2000). Molecular determinants that mediate selective activation of p38 MAP kinase isoforms. *EMBO J.* **19**, 1301–1311.
4. Wang, X. S., Diener, K., Manthey, C. L., Wang, S., Rosenzweig, B., Bray, J. *et al.* (1997). Molecular cloning and characterization of a novel p38 mitogen-activated protein kinase. *J. Biol. Chem.* **272**, 23668–23674.
5. Eckert, R. L., Efimova, T., Balasubramanian, S., Crish, J. F., Bone, F. & Dashti, S. (2003). p38 mitogen-activated

protein kinases on the body surface—a function for p38 delta. *J. Invest. Dermatol.* **120**, 823–828.
6. Hu, M. C., Wang, Y. P., Mikhail, A., Qiu, W. R. & Tan, T. H. (1999). Murine p38-delta mitogen-activated protein kinase, a developmentally regulated protein kinase that is activated by stress and proinflammatory cytokines. *J. Biol. Chem.* **274**, 7095–7102.
7. Shi, Y. & Gaestel, M. (2002). In the cellular garden of forking paths: how p38 MAPKs signal for downstream assistance. *Biol. Chem.* **383**, 1519–1536.
8. Lee, J. C., Laydon, J. T., McDonnell, P. C., Gallagher, T. F., Kumar, S., Green, D. *et al.* (1994). A protein kinase involved in the regulation of inflammatory cytokine biosynthesis. *Nature*, **372**, 739–746.
9. Han, J., Lee, J. D., Bibbs, L. & Ulevitch, R. J. (1994). A MAP kinase targeted by endotoxin and hyperosmolarity in mammalian cells. *Science*, **265**, 808–811.
10. Haq, R. & Zanke, B. (1998). Inhibition of apoptotic signaling pathways in cancer cells as a mechanism of chemotherapy resistance. *Cancer Metastasis Rev.* **17**, 233–239.
11. Harkin, D. P., Bean, J. M., Miklos, D., Song, Y. H., Truong, V. B., Englert, C. *et al.* (1999). Induction of GADD45 and JNK/SAPK-dependent apoptosis following inducible expression of BRCA1. *Cell*, **97**, 575–586.
12. Recio, J. A. & Merlino, G. (2002). Hepatocyte growth factor/scatter factor activates proliferation in melanoma cells through p38 MAPK, ATF-2 and cyclin D1. *Oncogene*, **21**, 1000–1008.
13. Lee, J. C., Kumar, S., Griswold, D. E., Underwood, D. C., Votta, B. J. & Adams, J. L. (2000). Inhibition of p38 MAP kinase as a therapeutic strategy. *Immunopharmacology*, **47**, 185–201.
14. English, J. M. & Cobb, M. H. (2002). Pharmacological inhibitors of MAPK pathways. *Trends Pharmacol. Sci.* **23**, 40–45.
15. Jackson, P. F. & Bullington, J. L. (2002). Pyridinylimidazole based p38 MAP kinase inhibitors. *Curr. Top. Med. Chem.* **2**, 1011–1020.
16. Kumar, S., Boehm, J. & Lee, J. C. (2003). p38 MAP kinases: key signalling molecules as therapeutic targets for inflammatory diseases. *Nat. Rev., Drug Discov.* **2**, 717–726.
17. Clerk, A., Michael, A. & Sugden, P. H. (1998). Stimulation of multiple mitogen-activated protein kinase sub-families by oxidative stress and phosphorylation of the small heat shock protein, HSP25/27, in neonatal ventricular myocytes. *Biochem. J.* **333**, 581–589.
18. Hazzalin, C. A., Cano, E., Cuenda, A., Barratt, M. J., Cohen, P. & Mahadevan, L. C. (1996). p38/RK is essential for stress-induced nuclear responses: JNK/SAPKs and c-Jun/ATF-2 phosphorylation are insufficient. *Curr. Biol.* **6**, 1028–1031.
19. Ono, K. & Han, J. (2000). The p38 signal transduction pathway: activation and function. *Cell Signalling*, **12**, 1–13.
20. Pugazhenthi, S., Boras, T., O'Connor, D., Meintzer, M. K., Heidenreich, K. A. & Reusch, J. E. (1999). Insulin-like growth factor I-mediated activation of the transcription factor cAMP response element-binding protein in PC12 cells. Involvement of p38 mitogen-activated protein kinase-mediated pathway. *J. Biol. Chem.* **274**, 2829–2837.
21. Xing, J., Kornhauser, J. M., Xia, Z., Thiele, E. A. & Greenberg, M. E. (1998). Nerve growth factor activates extracellular signal-regulated kinase and p38 mitogen-activated protein kinase pathways to stimulate CREB serine 133 phosphorylation. *Mol. Cell. Biol.* **18**, 1946–1955.
22. Kyriakis, J. M. & Avruch, J. (2001). Mammalian mitogen-activated protein kinase signal transduction pathways activated by stress and inflammation. *Physiol. Rev.* **81**, 807–869.
23. DeLano, W. L. (2002). *The PyMOL Molecular Graphics System.* DeLano Scientific, San Carlos, CA.
24. Zarubin, T. & Han, J. (2005). Activation and signaling of the p38 MAP kinase pathway. *Cell Res.* **15**, 11–18.
25. Ge, B., Gram, H., Di Padova, F., Huang, B., New, L., Ulevitch, R. J. *et al.* (2002). MAPKK-independent activation of p38alpha mediated by TAB1-dependent autophosphorylation of p38alpha. *Science*, **295**, 1291–1294.
26. Gills, J. J., Castillo, S. S., Zhang, C., Petukhov, P. A., Memmott, R. M., Hollingshead, M. *et al.* (2007). Phosphatidylinositol ether lipid analogues that inhibit AKT also independently activate the stress kinase, p38alpha, through MKK3/6-independent and -dependent mechanisms. *J. Biol. Chem.* **282**, 27020–27029.
27. Salvador, J. M., Mittelstadt, P. R., Guszczynski, T., Copeland, T. D., Yamaguchi, H., Appella, E. *et al.* (2005). Alternative p38 activation pathway mediated by T cell receptor-proximal tyrosine kinases. *Nat. Immunol.* **6**, 390–395.
28. Mittelstadt, P. R., Yamaguchi, H., Appella, E. & Ashwell, J. D. (2009). T cell receptor-mediated activation of p38α by mono-phosphorylation of the activation loop results in altered substrate specificity. *J. Biol. Chem.* **284**, 15469–15474.
29. Jirmanova, L., Sarma, D. N., Jankovic, D., Mittelstadt, P. R. & Ashwell, J. D. (2009). Genetic disruption of p38alpha Tyr323 phosphorylation prevents T-cell receptor-mediated p38alpha activation and impairs interferon-gamma production. *Blood*, **113**, 2229–2237.
30. Wilson, K. P., Fitzgibbon, M. J., Caron, P. R., Griffith, J. P., Chen, W., McCaffrey, P. G. *et al.* (1996). Crystal structure of p38 mitogen-activated protein kinase. *J. Biol. Chem.* **271**, 27696–27700.
31. Zhang, F., Strand, A., Robbins, D., Cobb, M. H. & Goldsmith, E. J. (1994). Atomic structure of the MAP kinase ERK2 at 2.3 Å resolution. *Nature*, **367**, 704–711.
32. Lee, T., Hoofnagle, A. N., Kabuyama, Y., Stroud, J., Min, X., Goldsmith, E. J. *et al.* (2004). Docking motif interactions in MAP kinases revealed by hydrogen exchange mass spectrometry. *Mol. Cell*, **14**, 43–55.
33. Tanoue, T., Adachi, M., Moriguchi, T. & Nishida, E. (2000). A conserved docking motif in MAP kinases common to substrates, activators and regulators. *Nat. Cell Biol.* **2**, 110–116.
34. Chang, C. I., Xu, B. E., Akella, R., Cobb, M. H. & Goldsmith, E. J. (2002). Crystal structures of MAP kinase p38 complexed to the docking sites on its nuclear substrate MEF2A and activator MKK3b. *Mol. Cell*, **9**, 1241–1249.
35. Galanis, A., Yang, S. H. & Sharrocks, A. D. (2001). Selective targeting of MAPKs to the ETS domain transcription factor SAP-1. *J. Biol. Chem.* **276**, 965–973.

36. Sheridan, D. L., Kong, Y., Parker, S. A., Dalby, K. N. & Turk, B. E. (2008). Substrate discrimination among mitogen-activated protein kinases through distinct docking sequence motifs. *J. Biol. Chem.* **283**, 19511–19520.
37. Canagarajah, B. J., Khokhlatchev, A., Cobb, M. H. & Goldsmith, E. J. (1997). Activation mechanism of the MAP kinase ERK2 by dual phosphorylation. *Cell*, **90**, 859–869.
38. Bell, M., Capone, R., Pashtan, I., Levitzki, A. & Engelberg, D. (2001). Isolation of hyperactive mutants of the MAPK p38/Hog1 that are independent of MAPK kinase activation. *J. Biol. Chem.* **276**, 25351–25358.
39. Avitzour, M., Diskin, R., Raboy, B., Askari, N., Engelberg, D. & Livnah, O. (2007). Intrinsically active variants of all human p38 isoforms. *FEBS J.* **274**, 963–975.
40. Diskin, R., Askari, N., Capone, R., Engelberg, D. & Livnah, O. (2004). Active mutants of the human p38alpha mitogen-activated protein kinase. *J. Biol. Chem.* **279**, 47040–47049.
41. Diskin, R., Engelberg, D. & Livnah, O. (2007). High-resolution diffracting crystals of intrinsically active p38alpha MAP kinase: a case study for low-throughput approaches. *Acta Crystallogr., Sect. D: Biol. Crystallogr.* **63**, 260–265.
42. Askari, N., Beenstock, J., Livnah, O. & Engelberg, D. (2009). p38alpha is active *in vitro* and *in vivo* when monophosphorylated at threonine 180. *Biochemistry*, **48**, 2497–2504.
43. Huse, M. & Kuriyan, J. (2002). The conformational plasticity of protein kinases. *Cell*, **109**, 275–282.
44. Taylor, S. J. & Shalloway, D. (1994). An RNA-binding protein associated with Src through its SH2 and SH3 domains in mitosis. *Nature*, **368**, 867–871.
45. Zhang, Y. Y., Mei, Z. Q., Wu, J. W. & Wang, Z. X. (2008). Enzymatic activity and substrate specificity of mitogen-activated protein kinase p38alpha in different phosphorylation states. *J. Biol. Chem.* **283**, 26591–26601.
46. Diskin, R., Lebendiker, M., Engelberg, D. & Livnah, O. (2007). Structures of p38alpha active mutants reveal conformational changes in L16 loop that induce autophosphorylation and activation. *J. Mol. Biol.* **365**, 66–76.
47. Bellon, S., Fitzgibbon, M. J., Fox, T., Hsiao, H. M. & Wilson, K. P. (1999). The structure of phosphorylated p38gamma is monomeric and reveals a conserved activation-loop conformation. *Structure*, **7**, 1057–1065.
48. Zhou, T., Sun, L., Humphreys, J. & Goldsmith, E. J. (2006). Docking interactions induce exposure of activation loop in the MAP kinase ERK2. *Structure*, **14**, 1011–1019.
49. Jacobs, D., Glossip, D., Xing, H., Muslin, A. J. & Kornfeld, K. (1999). Multiple docking sites on substrate proteins form a modular system that mediates recognition by ERK MAP kinase. *Genes Dev.* **13**, 163–175.
50. Murphy, L. O., Smith, S., Chen, R. H., Fingar, D. C. & Blenis, J. (2002). Molecular interpretation of ERK signal duration by immediate early gene products. *Nat. Cell Biol.* **4**, 556–564.
51. Murphy, L. O., MacKeigan, J. P. & Blenis, J. (2004). A network of immediate early gene products propagates subtle differences in mitogen-activated protein kinase signal amplitude and duration. *Mol. Cell. Biol.* **24**, 144–153.
52. Vinciguerra, M., Vivacqua, A., Fasanella, G., Gallo, A., Cuozzo, C., Morano, A. *et al.* (2004). Differential phosphorylation of c-Jun and JunD in response to the epidermal growth factor is determined by the structure of MAPK targeting sequences. *J. Biol. Chem.* **279**, 9634–9641.
53. Cowley, S., Paterson, H., Kemp, P. & Marshall, C. J. (1994). Activation of MAP kinase kinase is necessary and sufficient for PC12 differentiation and for transformation of NIH 3T3 cells. *Cell*, **77**, 841–852.
54. Dean, A. M., Lee, M. H. & Koshland, D. E., Jr (1989). Phosphorylation inactivates *Escherichia coli* isocitrate dehydrogenase by preventing isocitrate binding. *J. Biol. Chem.* **264**, 20482–20486.
55. Stura, E. A., Chen, P., Wilmot, C. M., Arevalo, J. H. & Wilson, I. A. (1992). Crystallization studies of glycosylated and unglycosylated human recombinant interleukin-2. *Proteins*, **12**, 24–30.
56. Otwinowski, Z. & Minor, W. (1997). Processing of X-ray diffraction data collected in oscillation mode. *Methods Enzymol.* **276**, 307–326.
57. Vagin, A. A. & Isupov, M. N. (2001). Spherically averaged phased translation function and its application to the search for molecules and fragments in electron-density maps. *Acta Crystallogr., Sect. D: Biol. Crystallogr.* **57**, 1451–1456.
58. Murshudov, G. N., Vagin, A. A. & Dodson, E. J. (1997). Refinement of macromolecular structures by the maximum-likelihood method. *Acta Crystallogr., Sect. D: Biol. Crystallogr.* **53**, 240–255.
59. Adams, P. D., Afonine, P. V., Bunkoczi, G., Chen, V. B., Davis, I. W., Echols, N. *et al.* (2010). PHENIX: a comprehensive Python-based system for macromolecular structure solution. *Acta Crystallogr., Sect. D: Biol. Crystallogr.* **66**, 213–221.
60. Morris, R. J., Perrakis, A. & Lamzin, V. S. (2003). ARP/wARP and automatic interpretation of protein electron density maps. *Methods Enzymol.* **374**, 229–244.
61. Emsley, P. & Cowtan, K. (2004). Coot: model-building tools for molecular graphics. *Acta Crystallogr., Sect. D: Biol. Crystallogr.* **60**, 2126–2132.